Available online at www.dergipark.org.tr/en

INTERNATIONAL ADVANCED RESEARCHES and ENGINEERING JOURNAL

Journal homepage: www.dergipark.org.tr/en/pub/iarej

e-ISSN: 2618-575X

International Open Access

Volume 05
Issue 03

December, 2021

Research Article

Dimensional optimization of two-phase flow boiling in microchannel heat sinks

Rahim Jafari [a,*]

[a] *Department of Automotive Engineering, Atilim University, Kızılcaşar St., İncek, Gölbaşı, 06830, Ankara, Turkey*

ARTICLE INFO

Article history:
Received 08 September 2021
Revised 28 November 2021
Accepted 10 December 2021

Keywords:
Electronics cooling
Microchannels
Mixture model
Optimization
Two-phase flow

ABSTRACT

The heat transfer coefficient (HTC) of microchannel heat sinks (MHS) is higher than common heat sinks due to higher area to volume ratio. Its value for two-phase flow boiling is much superior to single-phase flow. In addition, the two-phase flow boiling provides uniform wall temperature close to the coolant's saturation temperature in low vapor qualities. In the present study, a heat sink is optimized dimensionally after modeling of the boiling of R134a refrigerant in the microchannels. Firstly, mixture two-phase method along with the wall heat flux partitioning are utilized to introduce an applied thermal model to design MHSs. The heat sink mounted on the backside of an Intel core i7-900 desktop processor with dimensions of 19 mm×14.4 mm× 1 mm is numerically simulated to investigate the thermal performance. The HTC and the exit vapor quality are comparable with the available empirical correlations and first law of thermodynamics, respectively. Then the proposed model is developed to optimize the dimensions of the microchannels to design the heat sink with minimized wall temperature. Bound optimization by quadratic approximation (BOBYQA) method results in the optimized dimensions of the microchannels in the heat sink. Optimization of heat sink's geometry in terms of the dimensions of the microchannels at various boundary conditions will be practical as the unique application of the model.

1. Introduction

Dissipation of the generated excessive heat due to the increased power density is the major issue for compact integrated circuits. For instance, desktop PCs generated maximum heat flux of 108 W/cm^2 and maximum junction temperature of 85ºC in 2016 [1**Hata! Başvuru kaynağı bulunamadı.**]. In addition, the average power density for specialty applications such as laser diode arrays raised over 1000 W/cm^2 [2,3]. The conventional cooling methods such as forced air cooling in combination with heat sinks has maximum HTC of 250 W/m^2·°C [4]. Therefore, based on maximum junction temperature of 85°C and ambient temperature of 20°C, the dissipated heat flux typically limited to 20 W/cm^2 seems to be unsatisfactory to overcome this challenge.

MHS is an alternative method with a considerable and improved cooling capability for impacted electronic devices. HTC of MHSs is higher than common heat sinks due to higher area to volume ratio. Its value for two-phase flow boiling is much superior to single-phase flow. In addition, the two-phase flow boiling provides uniform wall temperature close to the coolant's saturation temperature except the higher vapor qualities near to one.

Available experimental data and correlations in the literature with adjustable parameters could be used to design MHSs with boiling. However, the results will be controversial issue as the parameters of interests fall outside the range of physical parameters, which they were developed. For instance, the mean absolute error of HTC for the correlation (smooth surface) suggested by Jafari et al. [5] has the minimum difference with the correlation proposed by Lee and Mudawar [6] and Kim and Mudawar [7]. The reason may be that the cooling fluid is R134a, which is the same for the first two correlations.

In addition, there are many numerical studies in the literature carried out to simulate flow boiling in microchannels. Common methods in the literature are based on the tracking of the interface between the liquid and vapor phases. Level-set method [8,9], Volume of Fluid [10], phase-field method [11,12] and Arbitrary Lagrangian-Eulerian (ALE) method [13] are techniques which track the interface of two separated phases of vapor and liquid. In Lattice- Boltzmann method, phase

* Corresponding author. Tel.: +90-312-586-8761; Fax: +90-312-586-8090.
E-mail addresses: rahim.jafari@atilim.edu.tr *(R. Jafari)*
ORCID: 0000-0003-1155-3711 *(R. Jafari)*
DOI: 10.35860/iarej.992871

separation occurs automatically and it is not necessary to track the interface [14]. It should be assumed that nucleation starts at a specified point like a tiny hot plate in a microchannel. All these methods have been employed to model different types of boiling flows as bubbly flow, slug flow, annular flow and film boiling in microchannels.

Türkakar and Okutucu-Özyurt optimized MHS mounted on Intel Core i7-900 Desktop Processor dimensionally for single phase [15] and two-phase flows [16]. Entropy generation analysis has been done to optimize the channels` dimensions.

Non-linear set of equations govern the two-phase flow. In addition, equations for interfacial discontinuity and mass transfer between the liquid and vapor phases make the model more complex. This way, local heat transfer and fluid flow properties such as the local HTCs and temperatures, bubble hydrodynamics in microscale and hot spots are predictable.

On the other hand, while the foregoing numerical methods provide precise information about the hydrodynamics and heat transfer of boiling in microscale, they are mostly restricted to confined geometries as a few bubbles, two-dimensional geometry and some presumptions due to computational time and cost. Therefore, an alternative numerical method, which is computationally cheaper than the aforementioned methods is required to simulate an extensive domain of MHSs. In the other words, an alternative quick and inexpensive model is necessitated to design MHSs, which phase change occurs. Besides, optimization of heat sink's geometry and boundary conditions will be practicable as the unique application of the method.

In the present study, the mixture method is utilized to develop a model, which results desired outcomes of saturated R134a flow boiling in MHSs in terms of HTC and vapor quality. An optimization is performed to minimize the temperature of the walls employing the proposed numerical method.

2. Numerical Model

2.1 Mixture Two-phase Flow Model

Mixture models [17] follow the average phase concentration, volume fraction, instead of the interface explicitly. Furthermore, one single momentum equation is defined to solve the mixture velocity, and both phases share the same pressure field. Hence, considerably smaller numbers of variables are solved comparing the other multiphase models. In this way, a multiphase model is developed for a practical application in which comprises whole geometry with less assumption.

The momentum equation for two phases is expressed as

$$\rho \frac{\partial u}{\partial t} + \rho(u \cdot \nabla)u = \nabla \cdot \left[-pI + \mu\left(\nabla u + (\nabla u)^T \cdot \frac{2}{3}(\nabla . u)I\right)\right] - \nabla . \left[\rho X(1-X) u_{slip} u_{slip}^T\right] + \rho g + F \quad (1)$$

where X and u_{slip} are the vapor quality and the relative velocity vector between two phases, respectively. The flow is assumed homogeneous and then the relative velocity between the phases is zero. Density and viscosity of two-phase flow are calculated with the volume averaged model as

$$\rho = \emptyset_l \rho_l + \emptyset_v \rho_v \quad (2)$$

$$\mu = \emptyset_l \mu_l + \emptyset_v \mu_v \quad (3)$$

A single continuity equation is written for the continuous (liquid) and dispersed (vapor) phases as:

$$(\rho_l - \rho_v)\left\{\nabla \cdot \left[\emptyset_v (1-X)\boldsymbol{u_{slip}}\right] + \frac{m_{lv}}{\rho_v}\right\} + \rho_l(\nabla \cdot \boldsymbol{u}) = 0 \quad (4)$$

m_{lv} is mass transfer rate from the liquid to the vapor. It is also related to the volume fraction of dispersed phase (ϕ_v) as:

$$\frac{\partial \emptyset_v}{\partial t} + \nabla \cdot \left\{\emptyset_v (\boldsymbol{u} + (1-X))\boldsymbol{u_{slip}}\right\} = -\frac{m_{lv}}{\rho_v} \quad (5)$$

The mass transfer rate is determined in terms of the transferred heat from the wall to the refrigerant for evaporation and the latent heat of the refrigerant as:

$$m_{lv} = \frac{Q_{evp}}{h_{fg}} \quad (6)$$

Same temperature is assumed for the liquid and vapor phases. In other words, the temperature of the fluid remains constant and it equals to the saturation temperature.

On the other hand, the temperature of microchannel walls rises as the heat is applied to the bottom wall of the heat sink. Hence there will be a discontinuity just at the walls of microchannels. To address this issue, new parameter is defined in which it consists of the saturation temperature in the fluid and the superheated temperature on the walls of the microchannel as boundary conditions. The temperature of walls are obtained by solving the energy equation for the heat sink as

$$\rho C_p \frac{\partial T}{\partial t} + \rho C_p u \cdot \nabla T + \nabla(-k\nabla T) = Q \quad (7)$$

2.2 Wall Heat Flux Partitioning

To determine the wall heat flux, numerous experimental and theoretical studies propose so-called heat partitioning which consists of three components of wall heat fluxes for low-pressure subcooled boiling flow [18-22]. The heat flux components include the single-phase turbulent convection, transient conduction due to the departing bubbles (quenching), and evaporation. Generally, the fluid flow in the microchannels is laminar and the effect of the turbulence is negligible. Moreover, available studies of the convective boiling in the literature concluded diverse outcomes in the microchannels. Some of the studies reported the dominance of the nucleate boiling in the microchannels [23,24]. Conversely, some other studies concluded the dominant mechanism is convective boiling [25,26]. In addition, the effect of the both of the nucleate and convective boiling mechanism has been reported [27,28]. Type of the boiling mechanism will result in different boiling flows as bubbly flow, slug flow, annular flow and film boiling in microchannels. Evaporation heat flux at the walls is calculated from [29]:

$$Q_{evp} = nf(\frac{\pi}{6}d^3)\rho_v h_{fg} \quad (8)$$

There are various correlations in the literature to predict the density of active nucleation sites, *n*, for pool boiling and fluid flow in macroscale [30-32]. It mostly depends on the wall superheat and surface parameters. Lemmert and Chwala [30] considered the wall superheat to correlate *n* as

$$n = [210(T_w - T_{sat})]^{1.805} \quad (9)$$

Benjamin and Balakrishnan [32] remarked *n* in terms of the wall superheat and the surface roughness as

$$n = 218.8Pr^{1.63}\left(\frac{1}{\gamma}\right)\theta^{-0.4}(\Delta T_{sat})^3 \quad (10)$$

Where θ and γ are calculated as

$$\theta = 14.5 - 4.5\left(\frac{R_a P}{\sigma}\right) + 0.4(\frac{R_a P}{\sigma})^2 \quad (11)$$

$$\gamma = \left(\frac{k_v \rho_v C p_v}{k_l \rho_l C p_l}\right)^{\frac{1}{2}} \quad (12)$$

Bubble departure frequency, *f*, is a complex function of the bubble formation process. Available studies in the literature concluded that the bubble departure frequency is a fluctuating parameter [33].

It is assumed that a bubble grows uniformly to the internal diameter of the microchannel before departing. Therefore, the model of Plesset and Zwick [34] to predict the bubble departure frequency is given as:

$$f = \left(\frac{\rho_l\, Cp_l \Delta T_{sat}}{\rho_v h_{fg} R}\right)^2 \frac{12\alpha_l}{\pi} \quad (13)$$

When a nucleated bubble grows, it departs from the surface and fresh fluid, comes into contact with the wall surface. The heated fluid by the transient conduction has been predicted by Mikic and Rohsenow [33] and the heat flux is considered as:

$$Q_q = \frac{2}{\sqrt{\pi}}\sqrt{f}\sqrt{k_l \rho_l C_{pl}} A_q (T_w - T_l) \quad (14)$$

where, A_q is expressed as

$$A_q = nK(\frac{\pi d^2}{4}) \quad (15)$$

K is a constant and is greater than unity. The heat flux due to the convection is calculated as:

$$Q_c = St\rho_l C_{pl} u_l (T_w - T_l)(1 - A_q) \quad (16)$$

Finally, the total wall heat flux, Q_w, is calculated as sum of evaporating, quenching and convection heat fluxes as:

$$Q_w = Q_{evp} + Q_q + Q_c \quad (17)$$

3. Geometry and Computational Domain

The viscosity effect on the lateral sides of the bubbles is neglected in 2D simulation; therefore, it would be less accurate than 3D. The computational domain is three-dimensional microchannel as depicted in Figure 1. In order to compare the simulation results with available experimental data in the literature, the computational domain and boundaries are defined same as the condition of the microchannel of heat sink experimented by Jafari et al. [5]. The height, width and length of the microchannel are 700 μm, 250 μm and 19 mm, respectively. Thermal properties of copper are used for the walls, except the top wall, which is assumed adiabatic. Coolant is refrigerant R134a with the inlet quality of 0.5 and the mass flux of 200 kg/m^2·s. The saturation temperature is 10ºC and it is assumed the outlet pressure remains at the saturation pressure. The thickness of the side walls is considered 53.5 μm which is half of the walls in the heat sink; hence, symmetry thermal boundary condition is applied to the outer sides of the walls. The initial and boundary conditions including the inlet quality and heat flux were selected respectively 0.5 and 20 W/m^2 to compare the results with the previous experimental study [5]. The dimensions of the heat sink and properties of the coolant are summarized in Table 1.

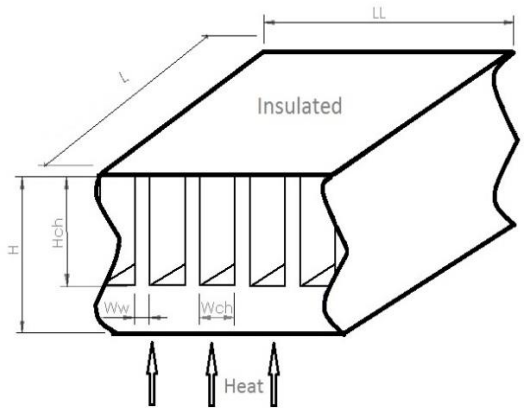

Figure 1. Heat Sink Geometry

Table 1. Dimensions of the heat sink and thermal properties of the refrigerant

Heat Sink		R134a	
L	19 mm	T_{sat}	10 ºC
LL	14.4 mm	h_{lg}	189.460 KJ/kg
H	1 mm	k_l	0.092 W/m·K
Microchannel		k_v	0.014 W/m·K
L	19 mm	μ_l	0.00024 Pa.s
W_{CH}	0.250 mm	μ_v	0.0000567 Pa.s
H_{CH}	0.700 mm	ρ_l	1261 kg/m^3
Applied Heat Flux	20 W/cm^2	ρ_v	23.74 kg/m^3
G	200 kg/m^2·s		

Since there is a little variation in the results by elapsing time, the steady-state solver failed. Therefore, the simulations have been conducted transient. A simulation has been implemented for applied base heat flux of 200 kW/m^2 for 5 seconds to distinguish the steady-state region. Table 2 illustrates number of meshes and sizes of the smallest grid. The grids sizes are determined finer in the domain of fluid than the solid part. Also, to take more accurate results at the corner of the microchannel, the smaller grids are distributed as well. The average wall temperature and average exit quality at different time steps are depicted in Figure 2 and Figure 3, respectively. It is obvious that after one second, the results converge to steady values. Furthermore, the results of meshing with four different mesh sizes are compared to evaluate the grid sizes on the outcomes.

Since the variation of the vapor quality is negligible for all the mesh sizes except the coarser mesh, the simulations are proceeded with coarse mesh to save the computational time and power.

Figure 4 illustrates the temperature and vapor quality distributions along the microchannel. Figure 4a shows that the temperature decreases from the bottom wall to the side walls of the microchannel about one kelvin. On the other hand, since the refrigerant temperature remains uniform at the saturation temperature along the microchannel specified by the blue color, temperature of the walls is nearly constant along the fluid flow, which is the advantage of the two-phase flow boiling comparing the single-phase flow. Based on the numerical model, it is assumed that the heterogeneous nucleation occurs on the walls of the microchannel. Therefore, the vapor quality rises along the microchannel. Figure 4b displays that the vapor quality increases gradually along the fluid flow as the saturated liquid gains heat from the walls and is converted to the saturated vapor.

Table 2. Number of grids for various meshing

Meshing	Number of tetrahedral elements	Minimum element quality (mm)
Coarser	204364	1.2× 10^{-3}
Coarse	395443	1.2× 10^{-3}
Fine	755271	0.16× 10^{-3}
Finer	998242	0.16× 10^{-3}

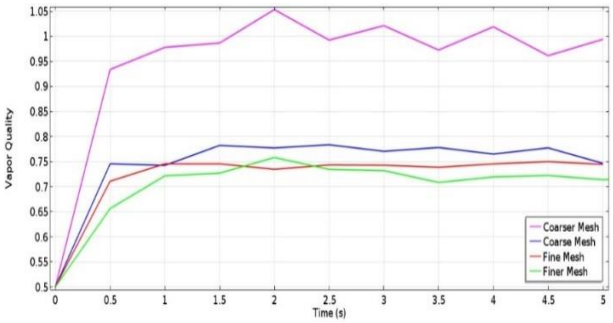

Figure 2. Variation of average wall temperature for two different sizes of grids by elapsing time ($\ddot{q}$ = 20W/cm^2)

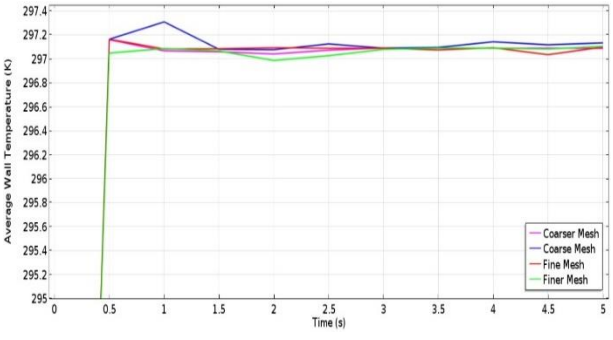

Figure 3. Variation of exit vapor quality for two different sizes of grids by elapsing time ($\ddot{q}$ = 20W/cm^2)

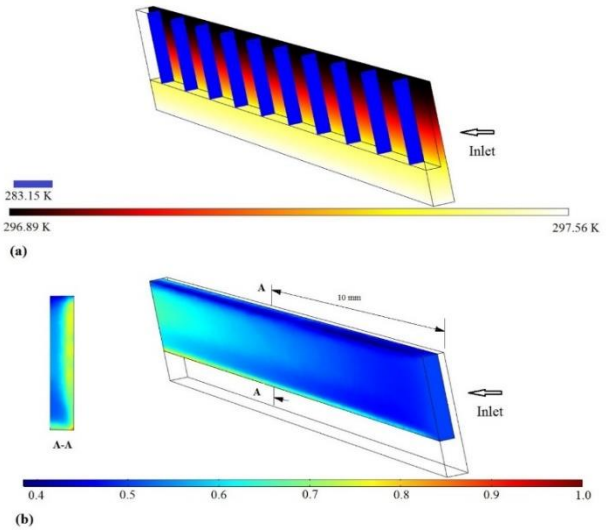

Figure 4. Temperature and (b) vapor quality distribution along the microchannel (Axisymmetric view)

4. Results and Discussion

4.1 Validation of the Numerical Model

The computational domain is selected such that determined in section 3. In addition, various heat fluxes from 5 W/cm^2 to 45 W/cm^2 have been applied to the base plane. This way, the initial and boundary conditions are identical with the conditions experimented by Jafari et al. [5]. Figure 5 illustrates the average HTC with respect to the applied base heat flux obtained with the present simulation and the experimental correlations available in the literature [5, 35-37].

The HTC grows strongly with increase of the corresponding heat flux. It is accordant with the experimental studies on the microchannels [39,40]. At low heat fluxes, the HTC of the present simulation and the experimental correlation of Kim and Mudawar [38] are in good agreement. The simulation results approached the experimental correlation of Lee and Mudawar [36] obtained from high heat fluxes as the applied heat flux grows. Since it has been assumed that bubbles nucleate uniformly along the walls and also the bubble departure diameter is restricted to the hydraulic diameter of the microchannel, the heterogeneous nucleate boiling is considered dominant in the simulations; however, based on the observation of the author from the previous experimental study [5] and also the captured flow patterns by Thiangtham et al. [41] for the applied ranges of heat flux, the dominant pattern in the experiments is annular flow. Therefore, employing of the proposed method to optimize the MHS with boiling flow at high heat fluxes will be much more realistic.

In order to evaluate the mass transfer from the liquid to the vapor, the average quality at the exit is calculated by first law of thermodynamics as:

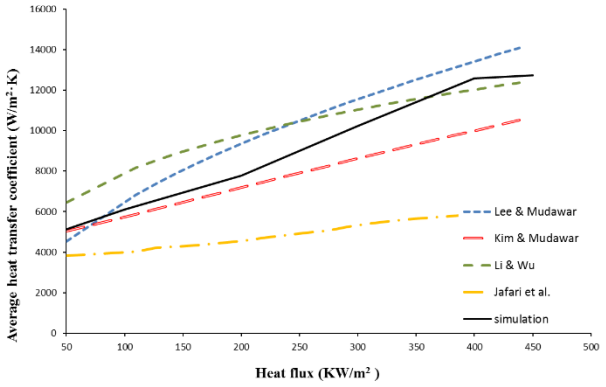

Figure 5. Comparison of the HTC between the experimental data and the proposed model

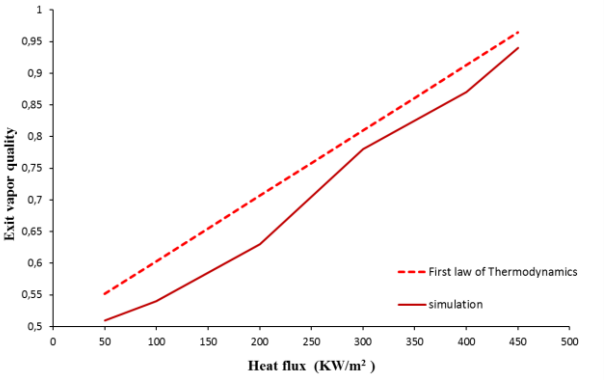

Figure 6. Comparison of exit vapor quality between the results of first law of thermodynamics and the present study

$$X_{out} = X_{in} + \frac{Q}{m_{lv} h_{fg}} \tag{18}$$

Figure 6 depicts the comparison of exit vapor quality with respect to the base heat flux between the simulation and Equation 18. The result shows a good agreement in the exit vapor quality between the simulation and the calculated values from Equation 18.

Although the length of the microchannels is some millimeters in the previous studies with phase-field method [10,11] and ALE method [12], the computational time of the proposed method is about one third of the phase-field method and half of the ALE method.

4.2 Optimization of the Geometry

The heat sink mounted on the backside of an Intel Core i7-900 Desktop Processor is considered for optimization. The overall dimensions of the heat sink are 19 mm×14.4 mm×1mm. The heat flux of 50 W/cm^2 is specified to be dissipated from the chip, which is a little greater than the actual generated heat (130 W). Two geometrical control variables, width and height of the microchannels, are used in the optimization. The optimization lower bound of the width and height are selected 100 μm. The lower bound is specified based on the manufacturing constraints. The upper bounds of the width and height are determined 500

μm and 700 μm, respectively. The upper limit of the width restricts the dimension to the microscale size. Besides, minimum thickness of 300 μm is considered to satisfy the strength of the bottom wall of the microchannel. The initial wall thickness of the microchannel is assumed constant and takes the value of 100 μm. This value is based on the manufacturing constraints to fabricate MHSs from copper using wire electro-discharge machining (WEDEM) [5]. The wall thickness would change a little due to obtain integer value for the number of the microchannels at each simulation. Initial and boundary conditions are stated in Table 3. The objective variable is determined the average walls temperature, which is interested parameter to minimize. Besides, the only property constraint is the exit vapor quality that should be less than 1 to assure the prevention of superheating in the microchannels.

The employed optimization method is BOBYQA, Bound Optimization BY Quadratic Approximation, which is an iterative algorithm to find a minimum of an objective function $F(x)$, $x \epsilon R^n$. It is subjected to specified bounds on the variables as $a_i<x_i<b_i$, $i = 1, 2, \ldots, n$, in which n refers to the number of variables. A quadratic approximation at the beginning of the k-th iteration has the form

$$Q_k(y_i) = F(y_i), \quad i = 1, 2, \ldots, m \tag{19}$$

m is a constant integer and equals $2n+1$. It is needed an initial control variable inside the specified bounds to begin the optimization. The interpolation points of first quadratic model (y_j $i = 1,2,\ldots,$m) are specified as

$$y_1 = x_0$$

$$y_{i+1} = x_0 + \Delta_1 e_i \text{ and } y_{n+i+1} = x_0 - \Delta_1 e_i \qquad a_i<(x_0)_i<b_i$$

$$y_{i+1} = x_0 + \Delta_1 e_i \text{ and } y_{n+i+1} = x_0 + 2\Delta_1 e_i \qquad (x_0)_i=a_i \tag{20}$$

$$y_{i+1} = x_0 - \Delta_1 e_i \text{ and } y_{n+i+1} = x_0 - 2\Delta_1 e_i \qquad (x_0)_i=b_i$$

where Δ_1 and e_i are the initial trust region radius and the i-th coordinate vector in R^n, respectively. The algorithm of the method is described in detail in references [42, 43] and the overall flowchart of the computational algorithm is represented in Figure 7.

Since just one of the microchannels of the heat sink is considered to be optimized, the misdistribution of the flow, which would lead temperature variation over the heat sink surface is ignored. The optimization is carried out for two sets of initial control variables. The results of the optimization for initial values of $H = 200$ μm, $W = 100$ μm and $H = 500$ μm, $W = 500$ μm are provided in Tables 4, 5, respectively. The results show that the minimum wall temperature equals 288.6 K and is obtained for the channels with width and height of 100 μm and 700 μm, respectively. Moreover, it is concluded that the optimized value does not change by varying the initial control variables. The optimization results are also employed to investigate the effects of the dimensional variations on the heat transfer and fluid flow parameters. Figure 8 shows the contour plots of the average wall temperature, average HTC, mass flow rate and exit vapor quality versus the width and height of the microchannels. It shows that the wall temperature decreases by increase of the aspect ratio (Height/Width). However, decrease in the average wall temperature does not comply with the increase in the average HTC.

Table 3. Dimensional ranges of microchannel and boundary conditions of optimization

Microchannels Height, μm	Upper bound	700
	Lower bound	100
Microchannels Width, μm	Upper bound	500
	Lower bound	100
Length, mm		14.4
Inlet quality		0.1
Mass flux, kg/m^2·s		500
Heat flux, KW/m^2		500
Saturation temperature, K		283.15

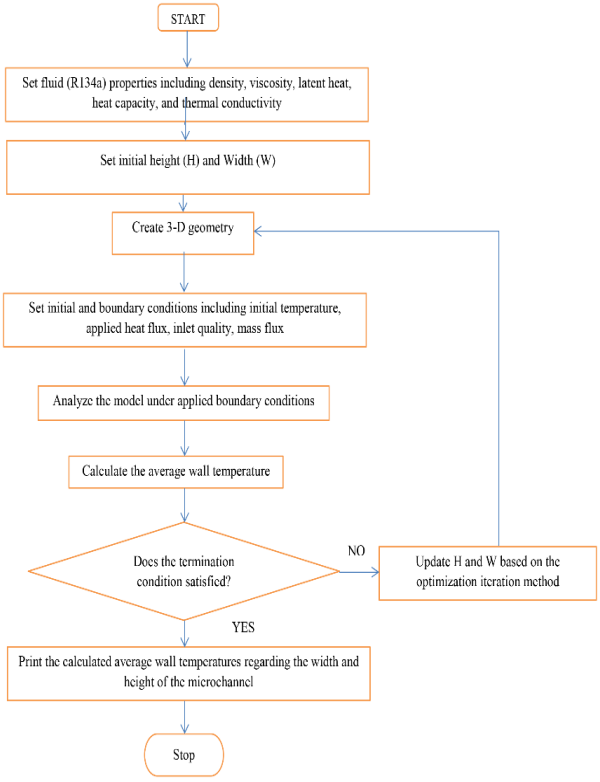

Figure 7. Flowchart of the computational algorithm

Table 4. Optimization results for q''= 50 W/cm^2, G = 500 kg/m^{2}s and initial W = 100 µm, H = 200 µm

Number	Width (µm)	Height (µm)	Width of walls (µm)	Number of channels	Ave. Walls temp. (K)	Mass flow rate (g/s)
1	100	200	98.9	95	295.3	0.95
2	140	200	99.2	79	298.0	1.10
3	100	240	98.9	95	293.5	1.14
4	180	200	102.0	67	299.3	1.20
5	100	160+	98.9	95	296.1	0.76
6	100	700	98.9	95	288.6	3.32

Table 5. Optimization results for q″= 50 W/cm2, G = 500 kg/m^{2}s and initial W = 500 µm, H = 500 µm

Number	Width (µm)	Height (µm)	Width of walls (µm)	Number of channels	Ave. Walls temp. (K)	Mass flow rate (g/s)
1	500	500	109.3	63	301.6	3.87
2	460	500	112.3	66	301.4	3.80
3	500	540	109.3	31	301.2	4.18
4	420	500	104.8	40	300.9	3.78
5	500	460	109.3	57	302.1	3.57
6	100	700	98.9	37	288.6	3.32

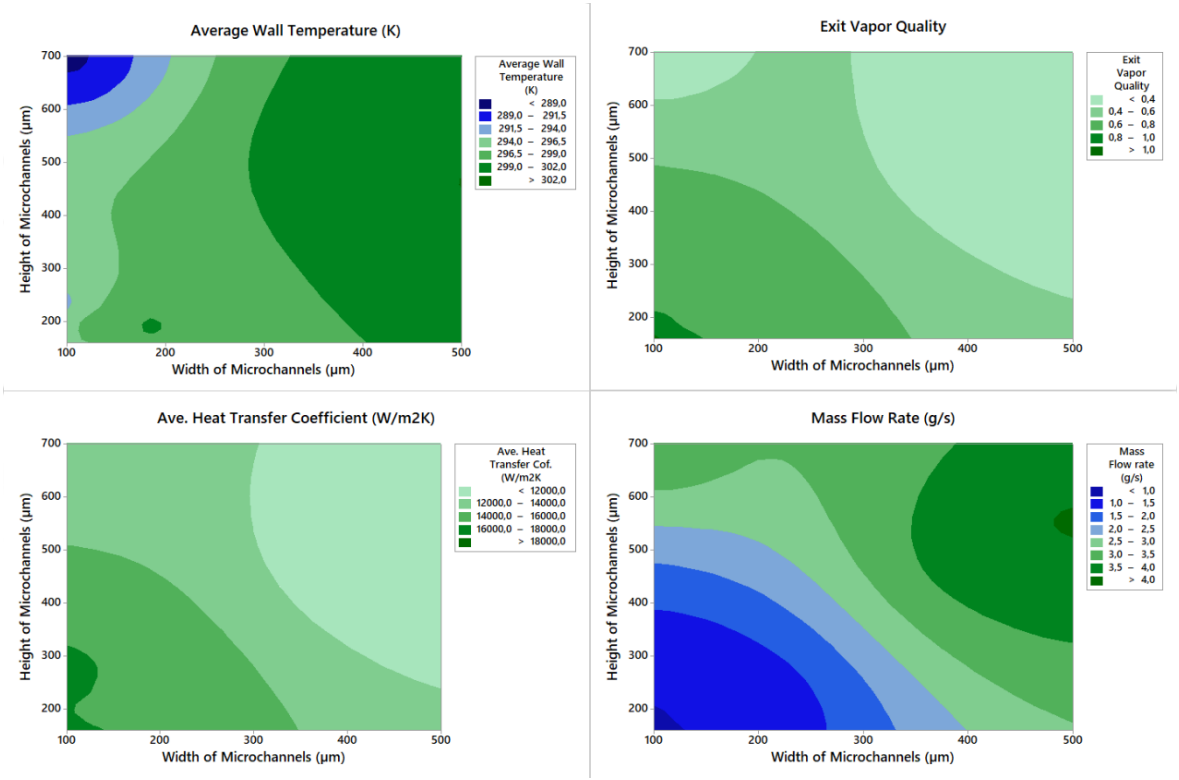

Figure 8. Contour plots of average wall temperature, average HTC, mass flow rate and exit vapor quality versus the width and height of the microchannels

Because of the reduction in applied heat to the walls of the microchannes, the exit vapor quality decreases as the sizes of the microchannels grow. The mass flow rate, which is proportional to the energy consumption by the compressor also rises by increment of microchannel size.

5. Conclusion

The mixture two-phase method along with the wall heat flux partitioning have been used to analyze two-phase flow boiling in MHSs. Intel Core i7-900 Desktop Processor has been considered as a heat source contained the overall area of 19mm × 14.4 mm and the maximum dissipated heat of 130 W. The average HTC and exit vapor quality have been determined according to the different applied heat fluxes. The HTC and the vapor quality rise by increasing the heat flux at the constant mass flux of G = 200 kg/m^2.s. The results have complied with the available experimental data and first law of thermodynamics. The constructed model has been extended to optimize the width and height of the microchannels for the maximum generated heat flux of 50 W/cm^2, which is a little more than the maximum generated heat flux from the aforementioned processor. The mass flux of 500 kg/m^2.s and the wall thickness of just about 100 µm have been supposed to be the constant values. The minimum wall temperature of 288.6 K has been gained for the maximum aspect ratio with the width and height of 100

μm and 700 μm, respectively. Türkakar and Okutucu-Özyurt also concluded that the channel height should be kept as high as the available volume permits. However, the average HTC restricts its value up to about 300 μm with the constant mass flux. The proposed model would be an appropriate method to optimize microchannels heat sinks dimensionally.

Declaration

The author(s) declared no potential conflicts of interest with respect to the research, authorship, and/or publication of this article. The author(s) also declared that this article is original, was prepared in accordance with international publication and research ethics, and ethical committee permission or any special permission is not required.

Author Contributions

All the numerical analysis, validation and writing of the article have been done by R. Jafari.

Nomenclature

A_q : Fraction of wall area cooled by quenching
C_p : Specific heat capacity, [J/kg·K]
D : Bubble departure diameter, [m]
f : Bubble departure frequency, [Hz]
$\boldsymbol{F}$: External forces vector, [N/m^3]
$\boldsymbol{G}$: Gravity acceleration vector, [m/s^2]
G : Mass flux [kg/m^2·s]
h_{lg} : Latent heat, [J/kg]
H : Height [m]
I : Identity matrix
K : Thermal conductivity, [W/m·K]
L : Length [m]
m_{lv} : Mass rate of evaporation, [kg/s]
n : Density of active nucleation sites
p : Pressure, [Pa]
Pr : Prandle number
R : Hydraulic diameter , [m]
Re : Reynolds number
$\boldsymbol{u}$: Velocity vector, [m/s]
W : Width [m]
X : Vapor quality
t : Time, [s]
T : Temperature, [K]
Q : Heat [W]
α : Thermal diffusivity, [m^2/s]
Δ : Radius of trust region, [m]
μ : Viscosity, [Pa·s]
ρ : Density, [kg/m^3]
σ : Surface tension coefficient, [N/m]
ϕ : Volume fraction
ch : Channel
l : Liquid
q : Quench
sat : Saturation
v : Vapor
w : Wall

References

1. Roadmap, IN, International Technology Roadmap for Semiconductors, 2006 Semiconductor Industry Association, 2009, http://www.itrs.net/ Last visited on August 30, 2015.
2. Krishnan, S., S. Garimella, G. Chrysler, and R. Mavajan, *Towards a thermal Moore's law*, IEEE Transactions on Advanced Packaging, 2007. **30**(3): p. 462-474.
3. Price, D. C., *A review of selected thermal management solutions for military electronic systems*, IEEE Transactions on Components and Packaging Technologies, 2003. **26**(1): p. 26-39.
4. Çengel, Y. A., and A. J. Ghajar, *Heat and mass transfer: fundamentals and applications*. 2014, McGraw-Hill Education.
5. Jafari, R., T. Okutucu-Özyurt, H. Ünver, and Ö. Bayer, *Experimental investigation of surface roughness effects on the flow boiling of R134a in microchannels*, Experimental Thermal and Fluid Science, 2016. **79**: p. 222-230.
6. Lee, J., and I. Mudawar, *Two-phase flow in high-heat-flux micro channel heat sink for refrigeration cooling applications Part II—Heat transfer characteristics*, International Journal of Heat and Mass Transfer, 2005. **48**(5): p. 941–955.
7. Kim, S.M., and I. Mudawar, *Universal approach to predicting saturated flow boiling heat transfer in mini/micro-channels – Part II. Two-phase heat transfer coefficient*, International Journal of Heat and Mass Transfer, 2013. **64**: p. 1239–1256.
8. Zhou, S., X. Xu, B.G., and Sammakia, *Modeling of boiling flow in microchannels for nucleation characteristics and performance optimization*, International Journal of Heat and Mass Transfer, 2013. **64**: p. 706–718.
9. Akhlaghi Amiri, H.A., and A.A. Hamouda, *Evaluation of level set and phase-field methods in modeling two phase flow with viscosity contrast through dual-permeability porous medium*, International Journal of Multiphase Flow, 2013. **52**: p. 22–34.
10. Zu, Y.Q., Y.Y. Yan, S. Gedupudi, T.G. Karayiannis, and D.B.R., Kenning, *Confined bubble growth during flow boiling in mini-micro-channel of rectangular cross-section part II: approximate 3-D numerical simulation*, International Journal of Thermal Sciences, 2011. **50**(3): p. 267-273.
11. Jafari, R., and T. Okutucu-Özyurt, *Phase-field modeling of vapor bubble growth in a microchannel*, Journal of Computational Multiphase Flows, 2015. **7**(3): p. 143–158.
12. Jafari, R., and T. Okutucu-Özyurt, *Numerical simulation of flow boiling from an artificial cavity in a microchannel*, International Journal of Heat and Mass Transfer, 2016. **97**: p. 270–278.
13. Jafari, R., and T. Okutucu-Özyurt, *3D numerical modeling of boiling in a microchannel by arbitrary Lagrangian–Eulerian (ALE) method*, Applied Mathematics and Computation, 2016. **272**: p. 596–603.
14. Gong, S., and P. Cheng, *Numerical investigation of saturated flow boiling in microchannels by the Lattice Boltzmann method*, Numerical Heat Transfer, 2014. **65**(7): p. 644–661.
15. Türkakar, G., and T. Okutucu-Özyurt, *Dimensional optimization of micro-channel heat sinks with multiple heat sources*, International Journal of Thermal Sciences, 2012.

62: p. 85–92.

16. Turkakar, G., T. Okutucu-Ozyurt, and S.G. Kandlikar, *Entropy generation analysis of a microchannel-condenser for use in a vapor compression refrigeration cycle*, International Journal of Refrigeration, 2017. **70**: P. 71–83.
17. Crowe, C., M. Sommerfeld, and Y. Tsuji, *Multiphase Flows with Droplets and Particles*, 1998. CRC Press.
18. Cooper, M.G, *The microlayer and bubble growth in nucleate pool boiling*, International Journal of Heat and Mass Transfer, 1969. **12**(8): p. 915–933.
19. Fath, H.S., and R.L. Judd, *Influence of system pressure on microlayer evaporation heat transfer*, ASME Journal of Heat Transfer, 1978. **100**(1): p. 49–55.
20. Victor, H., M. Del Valle, and D.B.R. Kenning, *Subcooled flow boiling at high heat flux*, International Journal of Heat and Mass Transfer, 1985. **28**(10): p. 1907–1920.
21. Hsu, Y.Y. and R.W. Graham, *Transport Processes in Boiling and Two-phase Systems*, 1976. Hemisphere, Washington, DC.
22. Graham, R.W., and R.C. Hendricks, *Assessment of convection and evaporation in nucleate boiling*, 1967. NASA TN D-3943.
23. Anwar, Z., B. Palm, and R. Khodabandeh, *Flow boiling heat transfer and dryout characteristics of R152a in a vertical mini-channel*, Experimental Thermal and Fluid Science, 2014. **53**: p. 207–217.
24. Bao, Z.Y., D.F. Fletcher, and B.S. Haynes, *Flow boiling heat transfer of freon R11 and HCFC123 in narrow passages*, International Journal of Heat and Mass Transfer, 2000. **43**(18): p. 3347–3358.
25. Qu, W., and I. Mudawar, *Flow boiling heat transfer in two phase microchannel heat sinks: I. Experimental investigation and assessment of correlation methods*, International Journal of Heat and Mass Transfer, 2003. **46**(15): p. 2755–2771.
26. Boye, H., Y. Staate, and J. Schmidt, *Experimental investigation and modelling of heat transfer during convective boiling in a minichannel*, International Journal of Heat and Mass Transfer, 2007. **50**(1): p. 208–215.
27. Lin, S., P.A. Kew, and K. Cornwell, *Flow boiling of refrigerant R141b in small tubes*, Transactions of the Institution of Chemical Engineers, 2001. **79**(A): p. 417–424.
28. McNeil, D.A., A.H. Raeisi, P.A. Kew, and R.S. Hamed, *Flow boiling heat-transfer in micro to macro transition flows*, International Journal of Heat and Mass Transfer, 2013. **65**: p. 289–307.
29. Bowring, R.W., *Physical model based on bubble detachment and calculation of steam voidage in the subcooled region of a heated channel*, Report HPR-10, Institute for Atomenergies, Halden, Norway, 1962.
30. Lemmert, M.,J., and J.M. Chwala, *Influence of flow velocity on surface boiling heat transfer coefficient*, in: E. Hahne, U. Grigull (Eds.), Heat Transfer in Boiling, Academic Press and Hemisphere, 1977. New York and Washington, DC.
31. Wang, C.H., and V.K. Dhir, *Effect of surface wettability on active nucleation site density during pool boiling of water on a vertical surface*, Journal of Heat Transfer, 1993. **115**(3): p. 659-669.
32. Benjamin, R.J., and A.R. Balakrishnan, *Nucleation site density in pool boilingof saturated pure liquids: effect of surface microroughness and surface and liquid physical properties*, Experimental Thermal and Fluid Science, 1997. **15**(1): p. 32-42.
33. Yoo, J., C.E. Estrada-Perez, and Y.A. Hassan, *A proper observation and characterization of wall nucleation phenomena in a forced convective boiling system*, International Journal of Heat and Mass Transfer, 2014. **76**: p. 568–584.
34. Plesset, M.S., and S. A. Zwick, *The growth of vapour bubble in superheated liquid*, Journal of Applied Physics., 1954. **25**(4): p. 493–500.
35. Mikic, B.B., and W.M. Rohsenow, *A new correlation of pool walking data including the fact of heating surface characteristics*, ASME Journal of Heat Transfer, 1969. **91**(2): p. 245–250.
36. Lee, J., and I. Mudawar, *Two-phase flow in high-heat-flux micro-channel heat sink for refrigeration cooling applications: Part II—heat transfer characteristics*, International Journal of Heat and Mass Transfer, 2005. **48**(5): p. 941–955.
37. Li, W., and Z. Wu, *A general correlation for evaporative heat transfer in micro/minichannels*, International Journal of Heat and Mass Transfer, 2010. **53**(9-10): p. 1778–1787.
38. Kim, S.M., and I. Mudawar, *Universal approach to predicting saturated flow boiling heat transfer in mini/micro-channels – Part II. Two-phase heat transfer coefficient*, International Journal of Heat and Mass Transfer, 2013. **64**: p. 1239–1256.
39. Agostini, B., J.R. Thome, M. Fabbri, B. Michel, D. Calmi, and U. Kloter, *High heat flux flow boiling in silicon multi-microchannels - Part I: Heat transfer characteristics of refrigerant R236fa*, International Journal of Heat and Mass Transfer, 2008. **51**(21-22): p. 5400-5411.
40. Bertsch, S., E.A. Groll, and S.V. Garimella, *Refrigerant flow boiling heat transfer in parallel micro channels as a function of local vapor quality*, International Journal of Heat and Mass Transfer, 2008. **51**(19-20): p. 4775-4787.
41. Thiangtham, P., C. Keepaiboon, P. Kiatpachai, L.G. Asirvatham, O. Mahian, A.S. Dalkilic, and S. Wongwises, *An experimental study on two-phase flow patterns and heat transfer characteristics during boiling of R134a flowing through a multi-microchannel heat sink*, International Journal of Heat and Mass Transfer, 2016. **98**: p. 390-400.
42. Powell, M.J.D., *The BOBYQA algorithm for bound constraint optimization without derivatives*, Report DAMTP 2009/NA06, University of Cambridge, UK.
43. Powell, M.D.J., *Developments of NEWUOA for minimization without derivatives*, IMA Journal of Numerical Analysis, 2008. **28**(4): p. 649-664.